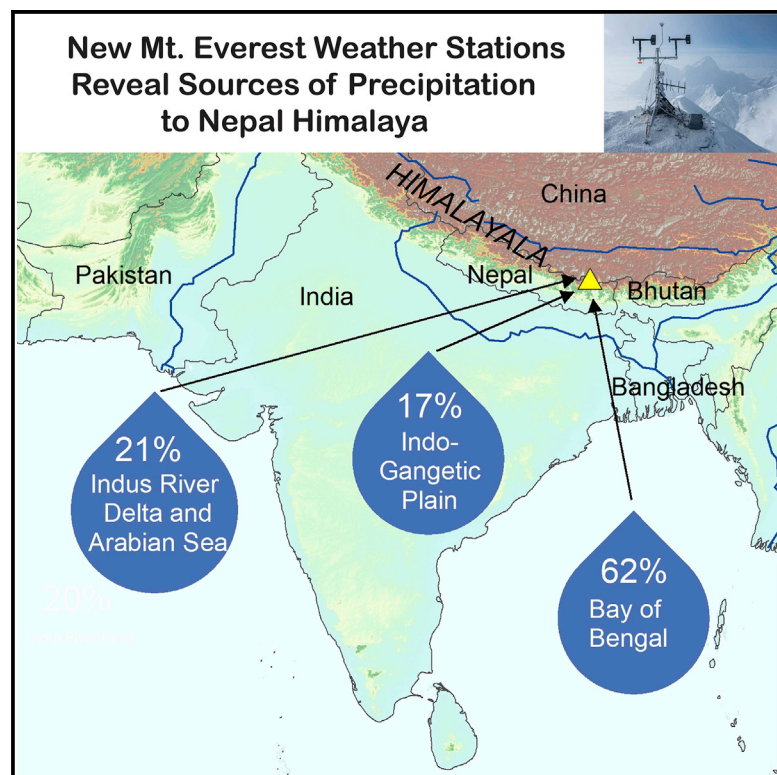


Precipitation Characteristics and Moisture Source Regions on Mt. Everest in the Khumbu, Nepal

Graphical Abstract



Authors

L. Baker Perry, Tom Matthews, Heather Guy, ..., Anton Seimon, Ananta Gajurel, Paul A. Mayewski

Correspondence

perrylb@appstate.edu

In Brief

Precipitation is critical to the water towers of the Hindu Kush-Himalaya-Karakoram region, exerting an important control on glacier mass balance and the water resources for 1.65 billion people. Here, we investigate precipitation characteristics and moisture sources in Nepal's Khumbu region. Our findings demonstrate that the northern Bay of Bengal is an important moisture source during the monsoon period (June to August) and that westerly trajectories over land predominate for precipitation events during the post-monsoon, winter, and pre-monsoon seasons.

Highlights

- Specific humidity and freezing level height have increased since 1981
- Bulk of precipitation falls during monsoon and at night
- Westerly trajectories predominate during post-monsoon, winter, and pre-monsoon
- Northern Bay of Bengal is an important moisture source during the monsoon period



Article

Precipitation Characteristics and Moisture Source Regions on Mt. Everest in the Khumbu, Nepal

L. Baker Perry,^{1,12,*} Tom Matthews,² Heather Guy,³ Inka Koch,^{4,5} Arbindra Khadka,^{5,6} Aurora C. Elmore,⁷ Dibas Shrestha,⁶ Subash Tuladhar,⁸ Saraju K. Baidya,⁸ Sunny Maharjan,⁸ Patrick Wagnon,⁹ Deepak Aryal,⁶ Anton Seimon,¹ Ananta Gajurel,¹⁰ and Paul A. Mayewski¹¹

¹Department of Geography and Planning, Appalachian State University, Boone, NC, USA

²Department of Geography and Environment, Loughborough University, Loughborough, UK

³School of Earth and Environment, University of Leeds, Leeds, UK

⁴Department of Geosciences, University of Tübingen, Tübingen, Germany

⁵International Centre for Integrated Mountain Development, Kathmandu, Nepal

⁶Central Department of Hydrology and Meteorology, Tribhuvan University, Kathmandu, Nepal

⁷National Geographic Society, Washington, DC, USA

⁸Department of Hydrology and Meteorology, Kathmandu, Nepal

⁹Université Grenoble Alpes, CNRS, Institute for Development Research, IGE, Grenoble, France

¹⁰Department of Geology, Tribhuvan University, Kathmandu, Nepal

¹¹Climate Change Institute, University of Maine, Orono, ME, USA

¹²Lead Contact

*Correspondence: perrylb@appstate.edu

<https://doi.org/10.1016/j.oneear.2020.10.011>

SCIENCE FOR SOCIETY Precipitation is the fundamental input to the water towers of Asia that sustain 1.65 billion people. In the Khumbu (Mt. Everest) region of the Nepal Himalaya, changing precipitation patterns have direct impacts on glacier behavior, local communities, and downstream populations. We use data from a new network of high-altitude weather stations to investigate precipitation amount and timing, and demonstrate that the northern Bay of Bengal is the main moisture source for the Khumbu during the monsoon period June–September. High-quality observations of precipitation at the highest elevations of the world’s water towers are critical for meeting the challenge of quantifying future availability of water resources for billions of people downstream.

SUMMARY

Precipitation is critical to the water towers of the Hindu Kush-Himalaya-Karakoram region, exerting an important control on glacier mass balance and the water resources for 1.65 billion people. Given that hydroclimatic extremes and water stress have emerged as key hazards in the context of climate change, Nepal’s Khumbu region overlaps key vulnerabilities. Here, we investigate the region’s precipitation characteristics and moisture sources through analysis of data from a new high-altitude network of automatic weather stations, which allows for a more complete understanding of the climatological precipitation data that are critical information for local communities in the Khumbu region, visitors, and downstream populations. Our findings demonstrate that the northern Bay of Bengal is potentially an important moisture source during the monsoon period (June to August) and that westerly trajectories over land predominate for precipitation events during the post-monsoon, winter, and pre-monsoon seasons.

INTRODUCTION

The Hindu Kush-Karakoram-Himalaya (HKH) are critical water towers for 1.65 billion people across Asia.^{1,2} Downstream communities suffer disproportionately from floods³ and are dependent on meltwater from seasonal snow and glacier ice, particularly during the pre-monsoon and drought periods.^{2,4–6} It

therefore causes concern that glacier loss has accelerated across the Himalayas in recent decades^{7,8} and that projections suggest large-scale reductions in stream discharge by 2050,^{6,9} yet more frequent episodes of intense precipitation.¹⁰ There is, however, much uncertainty about such projections, not least because of the limited understanding of the region’s contemporary hydroclimate. Precipitation is the largest freshwater input to



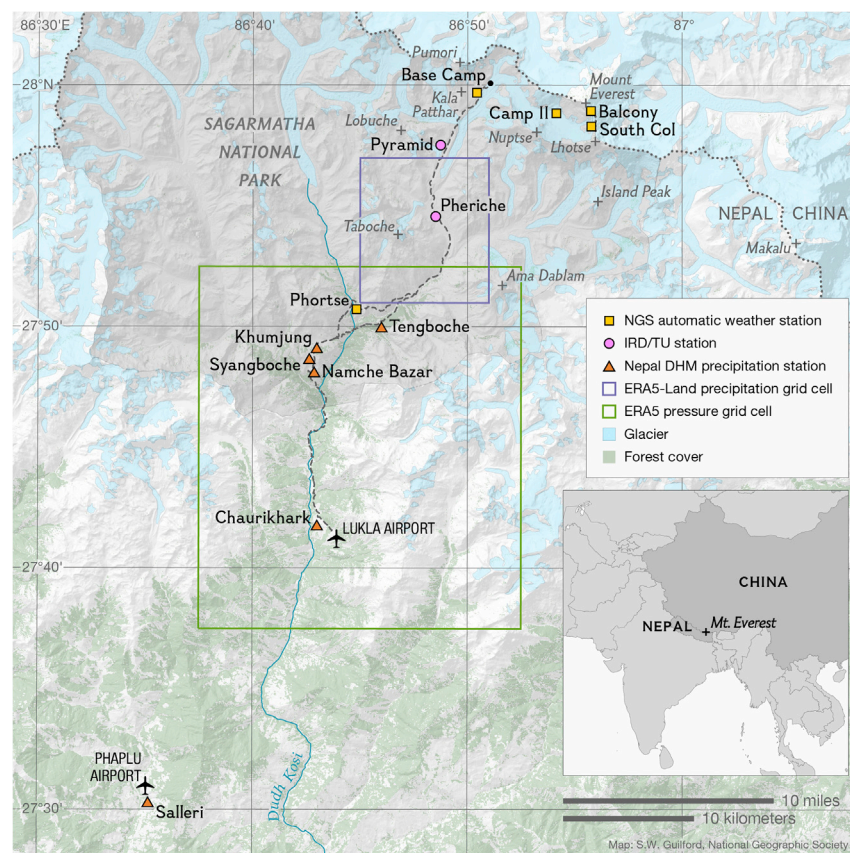


Figure 1. Khumbu Region Area of Study

Locations of precipitation data sources (filled squares, circles, and triangles) in the context of topography (shading), glacierized area (aqua shading), forest cover (green), and main trekking route to Everest Base Camp (dashes). The grid squares for ERA5 data presented are also shown (green and purple rectangles). Additional site location information is available in Table S5.

[asl]); however, it is not clear how regionally representative these findings may be. Considerable spatial variability in precipitation totals is similarly evident,²⁹ with positive altitudinal precipitation gradients on slopes with southerly exposure up to $\sim 3,000$ m^{30,31} and generally negative gradients above this elevation,²¹ albeit with considerable seasonal dependence,³² and some uncertainty between 3,600 and 5,000 m asl in the Khumbu region.²⁷ A pronounced altitude-independent south-north precipitation gradient of up to -21 mm km⁻¹ in the Khumbu region³³ and nearby Langtang³⁴ has been attributed to the shadowing effects of higher ridges and peaks. The orientation of this gradient is consistent with the southerly flow of the Bengal branch of the monsoon.^{33,35–39}

the glaciohydrological system in the HKH¹¹ and exerts a strong control over glacier mass balance,¹² but basic *in situ* measurements are lacking. For example, nearly all long-term observations of precipitation are from weather stations below 3,000 m, meaning that glacierized elevations have been largely unmonitored.^{13,14} As a result, precipitation amounts in these regions are poorly quantified,¹⁵ and understanding of key processes remains limited, leading to substantial uncertainties in future projections of climate, glacier mass balance, and water resource availability.¹⁶

Improving our knowledge of the precipitation climatology and key processes in the HKH is critical. Hydroclimatic extremes and water stress are emerging as key climate hazards there under global warming,^{1,17} placing mountain communities directly at risk. An in-depth assessment of precipitation in the Khumbu region in the central Himalaya (Figure 1) highlights some key vulnerabilities, as up to 56% of the domestic water supply for the more than 6,000 residents comes from rainwater,⁴ and locals and tourists alike suffer from precipitation extremes resulting in impassable and washed-out trails.¹⁸ Existing understanding identifies that precipitation across this region is subject to considerable temporal variability, with 70%–80% of annual totals falling during the summer monsoon period of June–September,^{19–21} when precipitation mostly falls at night.^{22–27} Ouyang et al.²⁸ report 50%–60% of annual precipitation falling during the monsoon in the Yadong Valley in the central Himalaya of China, with an afternoon peak in precipitation timing at higher elevations (>3,500 m above sea level

Wet periods during the monsoon are characterized by a deep mid-level (500 hPa) monsoon trough east of India and upper-tropospheric easterlies along the foothills of the Himalayas in association with the upper-level (200 hPa) Tibetan High.^{40,41} The largest direct contribution of moisture during heavy precipitation events in Nepal is the Indo-Gangetic Plain;⁴² a strong connection to the northern Bay of Bengal is evident during the monsoon period for Mt. Everest, known by its official names in Nepal and China as Sagarmatha and Qomolangma, respectively.⁴³ The abrupt end to monsoon precipitation by early October signals the transition to a much drier regime, although the remnants of land-falling tropical cyclones (TCs) infrequently impact the region with heavy precipitation resulting in landslides⁴⁴ and major flooding at lower elevations,^{45,46} as well as heavy snowfall^{33,47} and avalanches at higher elevations.^{48,49} Extratropical cyclones originating in the vicinity of the Caspian Sea and magnified by orographic effects produce the bulk of the precipitation in the winter (December, January, and February [DJF]) and result in a much shallower altitudinal gradient in precipitation.^{32,50} During the pre-monsoon season (March, April, and May [MAM]), convective activity—particularly on the higher ridges—becomes more common with a gradual moistening of the atmosphere.⁵¹

Secular changes to precipitation in Nepal have already been identified. A substantial reduction (47%) in precipitation during the monsoon period in the Khumbu region from 1994 to 2013 has been reported,²¹ while a mix of decreasing and increasing trends have been reported elsewhere in the eastern Himalaya and Nepal during June–September.^{10,52–54} The frequency of

extremely heavy precipitation events (i.e., >95th percentile) has also increased across portions of South Asia between 1951 and 2010⁵⁵ and intensification of various indices of precipitation extremes has recently been observed across Nepal.^{53,56} An increase in heavy precipitation coupled with rising freezing-level heights associated with elevation-dependent warming^{57–60} increases the flood threat in high-elevation glacierized basins, because rain is more likely to occur than snow.¹⁷ In fact, the probability of snowfall occurring on glacier fronts (at 4,817 m asl) decreased almost 11% between 1994 and 2013 in the Khumbu region.²¹ Future climate projections from Coupled Model Intercomparison Project Phase 5 (CMIP5) models indicate an increase in monsoon and winter precipitation by 2050 along with rising temperatures—especially in winter and at the highest elevations—in the Kosi River basin of Nepal, which includes the Khumbu region.⁶¹

Despite this existing research, the understanding of precipitation characteristics within the Khumbu region and its broader environmental impacts across the Nepal Himalaya remains tenuous. Interannual variability, observed trends, and seasonal cycles are uncertain above 3,500 m asl due to the numerous challenges of accurately measuring precipitation—particularly in its solid phase^{62,63}—combined with the limited number of high-elevation *in situ* measurements. These same challenges have limited characterization of the daily timing or phase of precipitation, which are critical influences on surface albedo and hence the energy balance of glacier surfaces.^{33,64} Although the Indo-Gangetic Plain and Bay of Bengal are recognized moisture sources for precipitation during the monsoon in portions of the region,^{42,43} the degree of altitudinal, seasonal, or synoptic dependence on these sources is unclear. Characterization of the vertical structure and physical processes associated with heavy precipitation in the Khumbu region is likewise limited, yet key to improving flood forecasts and various compound hazards, such as glacier lake outburst floods⁶⁵ and avalanches.

In this paper we analyze data from a new high-altitude network of automatic weather stations (AWSs) deployed in April and May 2019, as part of National Geographic and Rolex's Perpetual Planet Everest Expedition (hereafter 2019 Everest Expedition). Coupled with existing stations^{33,66} and regional-scale reanalyses, these data facilitate an event-level assessment of the physical processes associated with precipitation, enabling improved understanding of the potential impacts of climate warming on this critical component of the regional hydrological cycle. We use reanalysis data to place the AWS observations in context, but caution that the former are known to exhibit positive biases for precipitation over the Himalayas⁶⁷ and the adjacent Tibetan Plateau.^{68,69} Our specific objectives of this paper are to: (1) place the first complete year of precipitation observations from the new AWS network in a regional and longer-term context; (2) characterize the temporal patterns, intensity, and phase of precipitation across the region; (3) categorize moisture source regions and synoptic-scale circulation associated with precipitation; and (4) identify characteristics of heavy precipitation events.

Full details of the data and methods we use are provided in the Experimental Procedures. Briefly, we analyze long-term daily precipitation from Nepal Department of Hydrology and Meteorology (DHM) climate stations; moisture, temperature, and winds from ERA5 data; and hourly precipitation and other meteorolog-

ical parameters from the National Geographic Society (NGS) AWS network in the Khumbu region (Figure 1). The new AWS network¹³ complements an existing array of AWSs operated by the Institute for Development Research (IRD) and Tribhuvan University (TU),³³ and includes two comprehensive precipitation monitoring stations with weighing precipitation gauges and double alter windshields at Phortse (3,810 m asl) and Everest Base Camp (5,315 m asl). Three additional stations that are part of this new network are located above 6,000 m asl on Mt. Everest—Camp II (6,464 m asl), South Col (7,945 m asl), and Balcony (8,430 m asl)—and thereby provide an unprecedented dataset of *in situ* surface observations to characterize vertical profiles of temperature, moisture, and wind speed during precipitation events. For each precipitation event at Phortse, we used the Lagrangian particle dispersion model FLEXPART⁷⁰ (v.10.4) to simulate 72-h backward air trajectories that group into six clusters representing dominant moisture transport regimes using the NOAA HYSPLIT model trajectory clustering algorithm.⁷¹ We analyze low-, mid-, and upper-level flow patterns associated with each trajectory cluster by creating composite synoptic plots and analyze differences in *in situ* surface and ERA5 atmospheric parameters between heavy and light precipitation events.

RESULTS

Interannual Variability of Precipitation and Trends

Low interannual variability of monsoon and annual precipitation totals is evident, but precipitation in other seasons is more variable. We also note little trend in annual precipitation since 1981 for Chaurikhark (2,642 m asl), the longest continually operating climate station in the Khumbu region (Table S5). Some recent intensification in the hydroclimate is evident, with the three driest years occurring since 2008 (Figure 2A) and considerable interannual variability in heavy (>95th percentile) precipitation (Figure 2B). ERA5-Land mean annual precipitation for the upper Khumbu (Table 1, Figure 2C) is slightly greater than the calculated 3,000–4,000 m asl mean values and indicates positive trends in heavy (>95th percentile) precipitation ($p = 0.009$) since 1981 (Figure 2D). ERA5 June, July, August, and September (JJAS) freezing-level heights (Figures 2E) and 500 hPa specific humidity (Figure 2F) also indicate positive trends ($p < 0.001$) since 1981, with the former rising ~ 7 m year⁻¹ since 2005. Rising freezing-level heights indicate a higher frequency of liquid precipitation in glacier ablation zones and higher equilibrium line altitudes for glaciers, whereas increases in specific humidity suggest greater potential for heavy precipitation.

Observations of Precipitation in 2019–2020

Precipitation totaled 786 mm at Phortse (3,810 m) during the first year of observations of the NGS network, from 1 June 2019 to 31 May 2020, which is considerably less than the 942 mm mean annual precipitation for nearby long-term climate stations between 3,000 and 4,000 m. Monsoon (JJAS) precipitation accounted for 67% of the annual total at Phortse, compared with 76% according to climatology (Table 1). June 2019 was anomalously dry throughout the Khumbu region, with 25.8 mm at Phortse or $\sim 19\%$ of the climatological mean June precipitation for nearby stations (Table S1). Persistent precipitation in association with the 2019 monsoon did not arrive in Phortse until early July

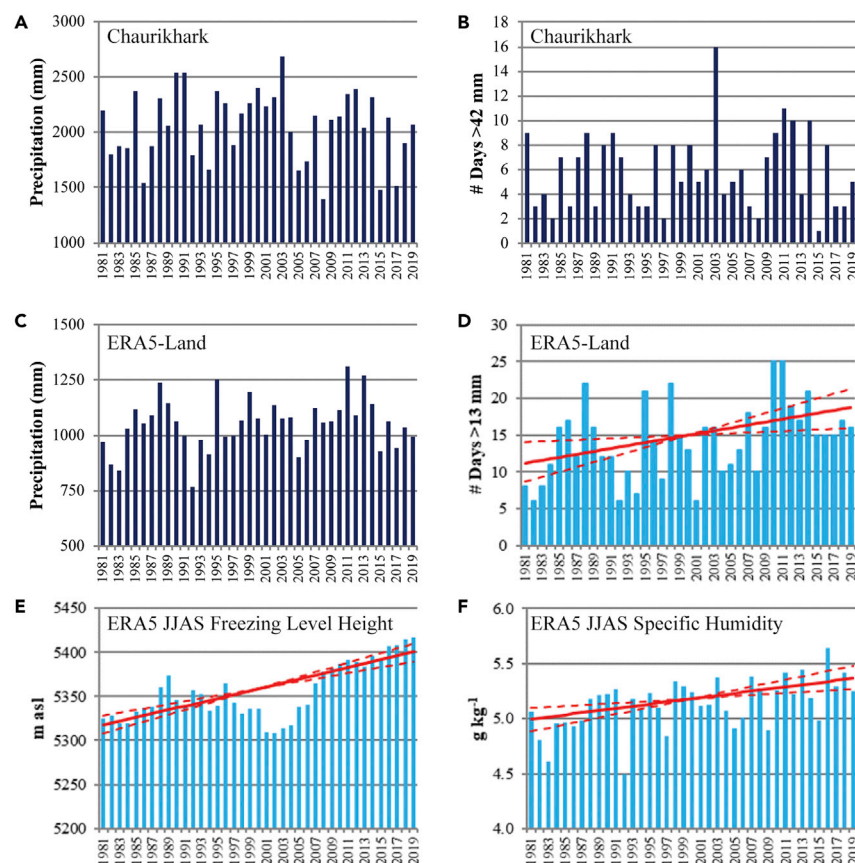


Figure 2. Interannual Variations in Precipitation and Moisture

(A and C) Annual precipitation totals and (B and D) number of days of heavy precipitation (>95th percentile) for (A and B) Chaurikhark and (C and D) ERA5-Land. Also shown are (E) ERA5 freezing level heights for monsoon (JJAS) and (F) ERA5 500 hPa specific humidity for monsoon (JJAS). The solid red line indicates the median Theil-Sen slope estimate, and the dotted red lines show the 5th–95th percentiles. Non-significant trends are not shown.

(Figure 3) and was marked by heavy rainfall (98.7 mm). The 2019–2020 winter season (DJF) was likewise highly anomalous, with 120.5 mm liquid equivalent (le) precipitation, all falling as snow, or 221% of the DJF climatological mean of nearby stations. Six snowstorms of >10 mm le precipitation (including 41.5 mm le from a 12–14 December 2019 storm) were observed along with persistent subfreezing temperatures and continuous snow cover from mid-December through mid-February. Recent (2016–2019) observations from Pheriche (4,260 m) and Pyramid (5,035 m) indicate 463 mm (17% snow) and 587 mm (23% snow) mean annual precipitation, respectively, with 76% of total precipitation falling during JJAS (Table 1).

Seasonal Cycles during Precipitation Events

Pronounced seasonal patterns emerge from an analysis of 2019–2020 precipitation events observed at Phortse, with most occurring during JJAS (60%) and MAM (26%) and the longest duration events in JJAS and DJF (Table S2). Mean event precipitation (mm/event) was highest in JJAS (5.1 mm) and DJF (9.3 mm). Phortse received the highest precipitation totals of all stations analyzed in all months except August 2019, when Pyramid recorded slightly more (Figure 4A). Mean temperatures during precipitation events at Phortse ranged from -4.9°C to 8.9°C from DJF to JJAS. Concurrent measurements at the other AWSs indicated that temperatures range between -20.7°C and -4.7°C at Camp II (6,464 m asl) and -32.7°C and -13.6°C at the South Col (7,945 m asl) (Figure 4B). The AWSs also indicate that wind speeds during Phortse precipitation events in JJAS

were relatively light up to 8,430 m asl on the upper reaches of Mt. Everest ($\leq 4.1\text{ m s}^{-1}$) and in the free troposphere (300 hPa; wind $\leq 7.4\text{ m s}^{-1}$), but increased substantially in DJF to 38.8 m s^{-1} at 300 hPa (Figure 4C). Such strong winds ultimately compromised the wind sensors at the Balcony and South Col in December (2019) and January (2020), respectively. Precipitable water and 500 hPa specific humidity are highest in JJAS and lowest in DJF (Figure 4D). Mean temperature lapse rates (see Experimental Procedures) between Phortse and Camp II are highest (i.e., less negative) in JJAS, consistent with abundant latent heat release during the monsoon, and lowest in DJF (Figure 4E). Estimated mean freezing-level heights

during precipitation events using observed lapse rates between Phortse and Camp II range from 2,915 m in DJF to 5,554 m asl in JJAS (Figure 4F), with values over 6,000 m asl during short-duration events in August 2019.

Daily Cycle of Precipitation

Detailed observations from Phortse (2019–2020), Pheriche (2016–2019), and Pyramid (2016–2019) indicate a distinct minimum in frequency during the late morning (0500–0700 UTC), followed by increasing frequency throughout the afternoon (Figures 5A, 5C, and 5E). Precipitation frequency peaks in the early evening ($\sim 1300\text{ UTC}$) at the higher stations of Pheriche and Pyramid and during the overnight hours (1800–2100 UTC) down valley at Phortse. Although most commonly observed during the monsoon, this daily pattern was also evident during other seasons at Phortse. Rain was the exclusive precipitation phase at Phortse and Pheriche in JJAS (Figures 5B and 5D). At Pyramid, all precipitation fell at air temperatures $>0^{\circ}\text{C}$ (rain or rain/snow mix) in JJA with increasing percentages of solid precipitation observed in September (Figure 5F). Heavily rimed snow particles (graupel) were observed primarily during the pre-monsoon in March and April at Phortse (Figure 5B), likely due to convective activity in association with higher concentrations of cloud liquid water.

Sources of Moisture

Moisture source regions inferred from 72-h FLEXPART backward trajectories for 2019–2020 precipitation events include

Table 1. Annual and Seasonal Climatological Precipitation Totals in the Khumbu Region

| Station | Mean Annual Precipitation (mm) | Standard Deviation | Coefficient of Variation | Percentage of Total Annual Precipitation by Season | | | |
|------------------------------|--------------------------------------|-----------------------|-----------------------------|--|--------------------------|--------------|--------------------------|
| | | | | Monsoon (JJAS) | Post- monsoon (ON) | Winter (DJF) | Pre- monsoon (MAM) |
| 2019–2020 Observations | | | | | | | |
| Phortse (3,810 m) | 786 | | | 67% | 2% | 15% | 16% |
| <i>Rain or mix (>0°C)</i> | 624 | | | 67% | 2% | 0% | 10% |
| <i>Snow/graupe! (≤0°C)</i> | 162 | | | 0% | 0% | 15% | 5% |
| Nepal DHM Stations | | | | | | | |
| Salleri (2,383 m) | 1,669 | 322 | 0.19 | 84% | 4% | 2% | 10% |
| Chaurikhark (2,642 m) | 2,101 | 417 | 0.20 | 85% | 3% | 2% | 10% |
| Namche Bazaar (3,450 m) | 992 | 238 | 0.23 | 74% | 8% | 7% | 10% |
| Syangboche (3,700 m) | 946 | 140 | 0.15 | 78% | 8% | 6% | 8% |
| Khumjung (3,750 m) | 831 | 142 | 0.17 | 76% | 6% | 6% | 12% |
| Tengboche (3,857 m) | 997 | 202 | 0.20 | 80% | 8% | 4% | 8% |
| 3,000–4,000 m mean | 942 | 181 | 0.19 | 77% | 8% | 6% | 10% |
| IRD/TU Stations | | | | | | | |
| Pheriche (4,260 m) | 463 | 62 | 0.14 | 76% | 2% | 5% | 16% |
| <i>Rain or mix (>0°C)</i> | 385 | 52 | 0.14 | 76% | 2% | 0% | 6% |
| <i>Snow/graupe! (≤0°C)</i> | 78 | 16 | 0.20 | 0% | 1% | 5% | 11% |
| Pyramid (5,035 m) | 587 | 34 | 0.06 | 76% | 2% | 6% | 17% |
| <i>Rain or mix (>0°C)</i> | 451 | 7 | 0.02 | 75% | 1% | 0% | 1% |
| <i>Snow/graupe! (≤0°C)</i> | 136 | 41 | 0.30 | 1% | 1% | 5% | 16% |
| ERA5-Land | | | | | | | |
| 27.9°N, 86.8°E grid | 1,050 | 116 | 0.11 | 77% | 5% | 7% | 12% |

Location information can be found in [Table S1](#).

the northern Bay of Bengal, Ganges and Brahmaputra river delta in Bangladesh, and Indo-Gangetic Plain in India. Important seasonal patterns are evident ([Figures 6A–6D](#)), with the Bay of Bengal effectively cut off during the non-monsoon seasons with more prevalent westerly trajectories. Results of the cluster analysis ([Figure 7A](#)) of the FLEXPART backward trajectories indicate that over half (56%) of all events are tied to the northern Bay of Bengal and Bangladesh (Clusters 1 and 3). The remainder of the clusters are associated with weak (Cluster 2) and moderate (Cluster 4) W flow (38%) and strong WNW flow (Cluster 5; 4%). All of the trajectory clusters are tied to ascent within 12 h of event maturation except for the subsidence noted in Cluster 5 ([Figure 7B](#)). Composite synoptic plots ([Figures S1–S3](#)), AWS observations, and ERA5 reanalysis data ([Table S3](#)) highlight the similarities between Clusters 1 and 3, characterized by the strong low-level Somali Jet across the Arabian Sea into the Indian subcontinent. Mid- and upper-tropospheric flow is quite weak in both clusters. Strong low-level SW flow over the Arabian Sea is also evident in Clusters 2 and 4, but mid- and upper-level W flow is much stronger in Cluster 4. Clusters 1, 2, and 3 are characterized by much higher precipitable water and mid- and upper-tropospheric moisture compared with Clusters 4 and 5 ([Table S3](#)).

Heavy Precipitation Events

Of the 171 precipitation events, heavy precipitation events ($>75^{\text{th}}$ percentile) during the monsoon were characterized by longer du-

rations associated with better moisture transport and higher mid- and upper-tropospheric relative humidity and specific humidity compared with light events ($<25^{\text{th}}$ percentile) ([Table S4](#)). Heavy events were also associated with 500 hPa ascent and shallower lapse rates. We note very little difference in mean temperature at all sites and levels, mean wind speeds at all sites and levels, or mean freezing-level heights between heavy and light events.

DISCUSSION

Long-Term Trends and Gradients in Precipitation

We observe no long-term trends in annual precipitation at Chaurikhark or in the ERA5-Land precipitation for the upper Khumbu ([Figures 2A and 2C](#)). This is in contrast to Salerno et al.,²¹ who found a 52% reduction in precipitation from 1994 to 2012 at Pyramid, although their findings were likely influenced (as they note) by poor data quality. The apparent discrepancy between no observed increase in annual precipitation ([Figures 2A and 2C](#)) and a highly significant trend in specific humidity ([Figure 2F](#)) during the monsoon is noteworthy and requires further investigation. Likewise, the general pattern of no observed increase in ERA5-Land annual precipitation ([Figure 2D](#)) coupled with an increase in extreme precipitation ([Figure 2D](#)) is consistent with projected increases under theoretical and projected climate scenarios.⁷⁴ Our reported significant rise in mean JJAS freezing-level height since 2005 ([Figure 2E](#))—with attendant impacts on precipitation

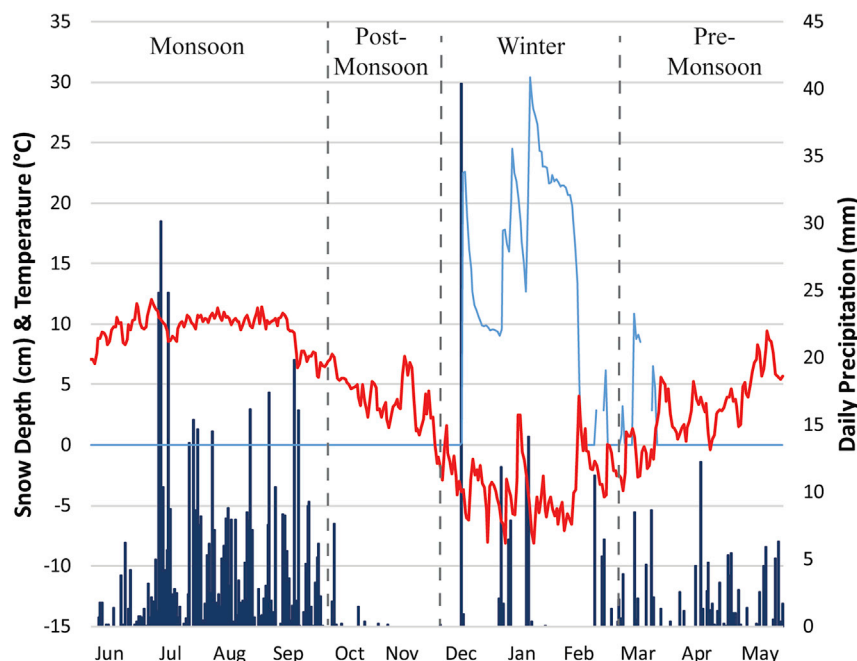


Figure 3. Meteorological Data from Phortse, Nepal

Observations from 1 June 2019 to 31 May 2020 at Phortse: mean daily temperature (red), snow depth (aqua), and daily precipitation total (blue bars).

phase and glacier accumulation—is likely a major factor in the acceleration of glacier retreat and thinning throughout the Khumbu region and broader HKH⁸ because of decreased accumulation and albedo feedback (e.g., rain results in lower albedo and enhanced absorption of short-wave radiation).

The wider network of operational AWSs (IRD/TU stations at Pheriche and Pyramid), longer-term DHM climate stations, and reanalysis datasets enable important aspects of the variability across space and time to be analyzed. An altitudinal and south-north gradient in precipitation is evident from the longer-term DHM datasets, which are generally consistent with previous studies,²¹ with an ~50% reduction in precipitation moving from Chaurikhark to Namche Bazaar, further decreasing upslope to Syangboche and Khumjung (Table 1). The relationship becomes more complex in the upper Khumbu region due to terrain shadowing and is not consistent with the findings of Salerno et al.²¹ that indicate negative altitudinal gradients in precipitation throughout the upper Khumbu; our analyses show that Pyramid (5,035 m asl) reported consistently higher precipitation totals than Pheriche (4,260 m asl) during 2016–2019. This discrepancy may partially result from inaccurate precipitation measurements, especially for solid precipitation;⁶³ we report that more recent (2016–2019) mean annual precipitation data from a shielded weighing precipitation gauge (587 mm; Table S1) are considerably higher than totals reported from an unshielded and unheated tipping bucket (449 mm) at Pyramid (1994–2012).²¹ In general, our measurements of precipitation by season are in excellent agreement with previous studies in the Khumbu²⁷ and in the broader Nepal Himalaya,^{6,19,20} with 75%–80% of the annual precipitation on average falling during the monsoon.

2019–2020: An Unusual Year

Spanning 3,800–8,430 m asl, the NGS AWS network provides an opportunity to improve our understanding of precipitation in the Khumbu region of Nepal. It enables insight into the processes

driving precipitation at the heart of the Himalayan water tower, of vital importance to local residents and the environment and communities downstream. Measurements from the network indicate that the observed climatic conditions during its first year of operation were unusual. The 786 mm total precipitation between 1 June 2019 and 31 May 2020 in Phortse was considerably less than the climatological mean precipitation for nearby stations at similar elevations, despite an exceptionally snowy winter. The anomalously low annual precipitation may be tied to the delay in the 2019 monsoon onset across eastern Nepal,⁷⁵ resulting in only 19% of

mean June precipitation in Phortse and the driest June on record since at least 1981 in Chaurikhark. Indeed, the 2019 monsoon did not arrive in the Khumbu until early July.^{13,76} Despite the paucity of long-term records of snowfall and snow depth across the Khumbu, it is apparent that the six major snowstorms of >10 mm le, 120.5 mm total precipitation, and nearly continuous snow cover during DJF were highly anomalous. The DJF Phortse precipitation totals were also considerably more than the climatological mean precipitation from nearby stations (54.7 mm) as well as Pyramid (32.3 mm). Although the presence of nearly continuous high-elevation winter snow cover is relatively common in other parts of Nepal (e.g., Ganja La Pass at 4,962 m asl in Langtang⁷⁷), it is not typical in the upper Khumbu region and has important implications for winter grazing, soil processes, and tourism.

Precipitation Totals and Phase by Season

Timing of precipitation at the seasonal timescale has an important influence on precipitation phase and attendant consequences for glacier mass balance. We find that rain predominates even at Pyramid (5,035 m asl) during the monsoon, largely consistent with the results of Salerno et al.²¹ In contrast, however, our analysis identifies that a rain/snow mix does occur at Pyramid, even in July and August, suggesting that freezing-level heights during precipitation do routinely fall to ~5,300 m asl (i.e., within ~300 m of Pyramid using derived lapse rates). Frequency of graupel precipitation peaks in March–April at Phortse and appears to be consistent with an increase in the pre-monsoon convective activity⁵¹ and weaker altitudinal gradients in precipitation³² across the Nepal Himalaya. The increase in pre-monsoon contributions to annual precipitation from 10% at Chaurikhark (2,642 m asl) to 17% at Pyramid (5,035 m asl) is noteworthy and broadly consistent—although reduced in magnitude—with the relatively greater importance of the pre-monsoon precipitation at higher elevations in the Yadong Valley.²⁸

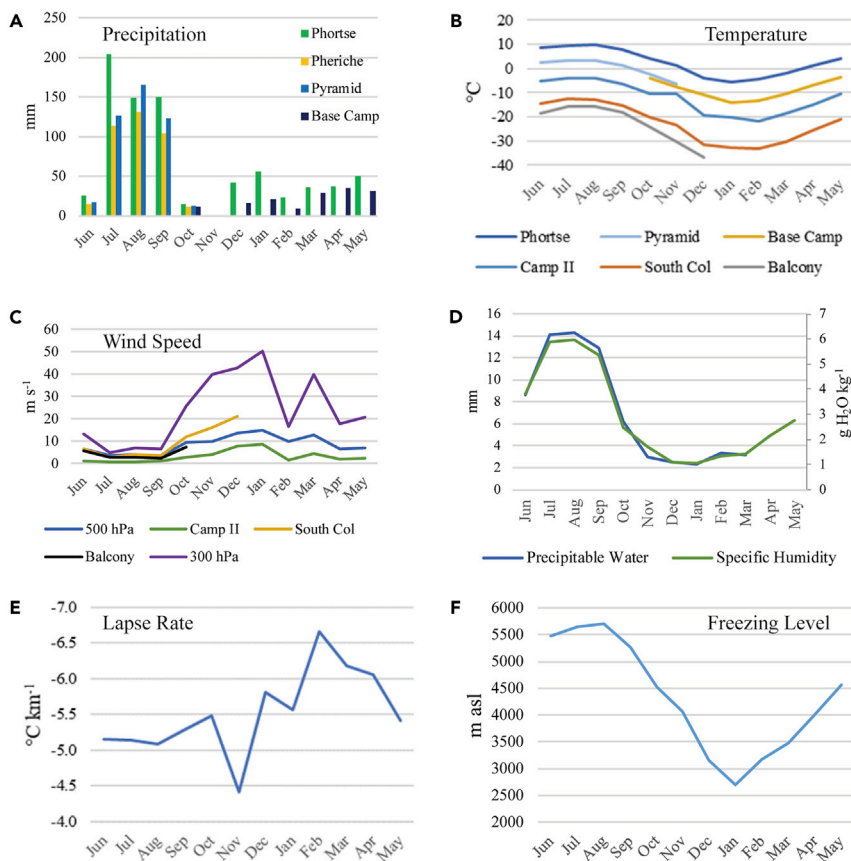


Figure 4. Phortse Precipitation Characteristics

Monthly characteristics of 171 precipitation events at Phortse observed during 2019–2020. (A) Total precipitation at Phortse (green), Pheriche (orange), Pyramid (light blue), and Base Camp (dark blue); (B) mean temperature; (C) mean wind speed; (D) ERA5 mean precipitable water (blue) and specific humidity (green); (E) mean temperature lapse rate between Phortse and Camp II; and (F) mean freezing-level height calculated from (E). Precipitation data available at Pheriche and Pyramid only from 1 June 2019 to 20 November 2019 and at Everest Base Camp from 10 October 2019 to 31 May 2020.

Lagrangian air mass tracking. We found that moisture source regions during the post-monsoon, winter, and pre-monsoon were quite distinct from the monsoon, with westerly trajectories predominating from October to May, and southerly flows more frequent in the monsoon. This could manifest as a seasonal pattern in vertical precipitation gradients, as it has been noted elsewhere that westerly circulation does not exhibit as substantial a decline in precipitation amounts at high altitude as is observed for monsoonal air masses.^{6,50,83}

Although our results indicate that the precipitation gradient between the lower

and the upper Khumbu region was lowest in August and April (Figure 4A), inconsistent data availability from Pheriche, Pyramid, and Everest Base Camp prevents a complete assessment of seasonal variability of vertical precipitation gradients or the altitudinal dependence of moisture source regions at this stage. However, we note very little variability in backward air trajectories for air parcels between 650 and 400 hPa for heavy precipitation events during the monsoon, thereby suggesting minimal altitudinal variability in moisture source regions.

The backward trajectories also hint at moisture provenance during precipitation events, and the northern Bay of Bengal emerged as a particularly important potential source region in our assessment. Variability in sea surface temperatures (SSTs) here may therefore be an important influence on precipitation rates in the Khumbu, given that Matthews et al.⁸⁴ have shown that atmospheric moisture content at the site of precipitation is correlated with SSTs in the source region; and in our results we noted that heavy precipitation events in the Khumbu region were associated with higher specific humidity. We therefore speculate that modes of climate variability that influence SSTs in the northern Bay of Bengal⁸⁵ may in turn relate to precipitation intensities in the Khumbu region, assuming similar tropospheric stability profiles. The inferred connections between westerly Clusters 2 and 4 (Figure 7A) and land moisture sources over the Indo-Gangetic Plain also highlight the potential impacts of land use/land cover change and/or irrigation⁸⁶ on evapotranspiration.

Daily Cycle of Precipitation

An understanding of the physical processes driving precipitation is critical for interpreting observed trends and estimating likely future changes. In this context, we observe that precipitation occurrence exhibits a nighttime peak (Figures 5A, 5C, and 5E), which is consistent with other locations across the central Himalaya,^{22–26,28} and in general agreement with previous findings from the Khumbu.⁴⁹ Our results indicate that the peak precipitation frequency occurs near or shortly after mean sunset at Pyramid and Pheriche (~1300–1430 UTC) and just after local midnight (~2100 UTC) at Phortse. Although the physical mechanisms driving this nighttime maximum remain speculative, several studies have suggested that convergence between prevailing upslope flow with downslope katabatic mountain breezes (driven by nocturnal radiative cooling) plays an important role in triggering the nighttime precipitation during moist periods.^{23–26} This hypothesis is consistent with our results that indicate precipitation frequency peaking at the higher station (Pyramid) earliest, progressing down valley to Pheriche, and then ~6 h later peaking at the lowest station (Phortse). Other nighttime maxima in precipitation frequency have also been reported in the tropical Andes of Peru and Bolivia^{72,78,79,80} and other high mountain regions,^{81,82} suggesting potential similarity in physical processes that warrants further investigation.

Event-Scale Processes and Moisture Source Regions

Further insights into the physical processes driving precipitation were provided with the event-level analysis, including

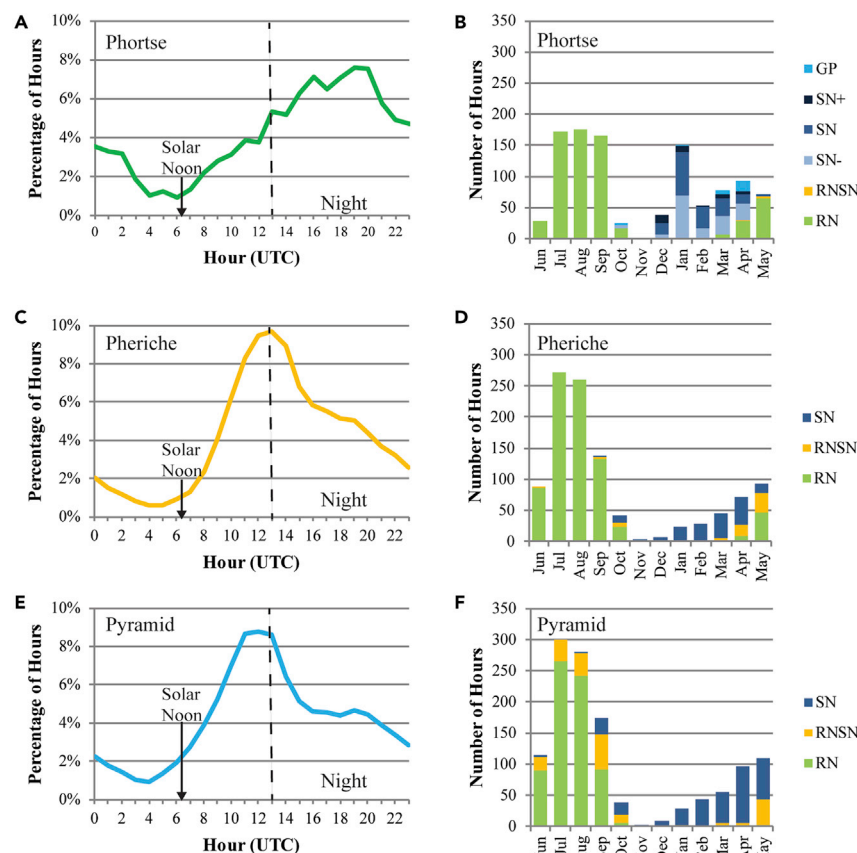


Figure 5. Timing and Phase of Precipitation

Daily timing of precipitation (>0.1 mm) and number of hours of precipitation by phase/intensity (Abbreviations are as follows: GP, graupel; SN+, heavy snow; SN, moderate snow; SN-, light snow; RNSN, rain/snow mix; RN, rain) for each month at (A and B) Phortse, (C and D) Pheriche, and (E and F) Pyramid. Dashed line in (A), (C), and (E) corresponds to mean sunset. Precipitation phase/intensity at Phortse were determined by OTT Parsivel² and precipitation phase at Pheriche and Pyramid was determined using air temperature following Forland et al.⁷² and applied to tropical mountain environments.⁷³ Phortse data are for 1 June 2019 to 31 May 2020; Pheriche and Pyramid data are for 27 May 2016 to 20 November 2016.

associated with TC Fani (3–5 May 2019) did impact the region during the installation fieldwork, resulting in 11.4 mm precipitation at Pyramid, as did TC Ampham (11.3 mm at Base Camp and 13.1 mm at Phortse 19–21 May 2019). The remnants of TC Nisarga provided a more substantial impact from 4 to 6 June 2020, with 35 mm le snow precipitation falling at Everest Base Camp and 46 mm rain in Phortse. Despite CMIP5 projections of increased (decreased) TC frequency in the Arabian Sea (Bay of Bengal),⁹⁰ the precipitation totals associated with landfalling TCs are projected to increase in coming decades,^{91,92} and extreme snowfall, avalanches, landslides,

We identified mid- and upper-level relative humidity, mid-level moisture content, and mid-level ascent as key ingredients necessary for heavy precipitation to develop over the Khumbu region. The presence of a deep moist layer extending above 8,000 m asl appears to be an important factor in the formation and persistence of heavy precipitation and is consistent with vertically pointing radar observations from Everest Base Camp during a pre-monsoon snowstorm that indicated highest radar reflectivity occurring in association with higher echo top heights.⁸⁷ Shallower lapse rates during heavy precipitation are more likely a product of latent heat release associated with higher moisture content.⁷⁶ Despite CMIP5 model projections of increased precipitation in the upper reaches of the Koshi basin,⁶¹ the strongly negative mass balance in glacier ablation zones associated with rising freezing levels, and likely compounded by the increased latent heat release and higher specific humidity, is almost certain to counteract any positive mass balance from increasing snowfall in accumulation zones. We stress, however, that a number of future scenarios of precipitation across the region are possible and could also be affected by anthropogenically emitted black carbon⁸⁸ and land surface change⁸⁹ across the Indian subcontinent.

Tropical Cyclone Impacts

We observed peripheral effects, but no major impacts, in the Khumbu region associated with TCs during our first complete year of observations from the new NGS AWS network. Moisture

and flooding are all emerging risks in the Khumbu.¹⁷ Robust observational networks and improved weather forecasting are critical to prevent a repeat of the substantial death toll that occurred in the Annapurna region associated with the remnants of TC Hudhud in October 2014.⁴⁸ Of even greater relevance is the poorly forecast November 1995 TC that had major impacts in the Khumbu region: 24 died from an avalanche in Gokyo, with 2 m of snowfall reported near Pheriche.⁹³

Caveats, Limitations, and Summary

Several caveats and limitations of this study merit discussion. First, the absence of high-quality precipitation observations over longer periods (>10 years) at elevations above 3,500 m asl in the Khumbu region and in most other parts of the HKH region substantially limits understanding of climatological patterns and trends. How to sustain and expand these critical high-elevation networks over the long term is a fundamentally important question that will require substantial international, interdisciplinary, and interinstitutional collaboration. Second, our analysis was largely restricted to the first year of the newly installed NGS AWS network, and some periods of missing data from Pheriche, Pyramid, and Everest Base Camp precluded a more complete characterization of the vertical and south-north precipitation gradients. Third, our Lagrangian assessment infers moisture source regions only through 72-h backward air trajectories and does not explicitly quantify where it originates (i.e., where evaporation occurs⁹⁴). Future research is therefore needed to physically

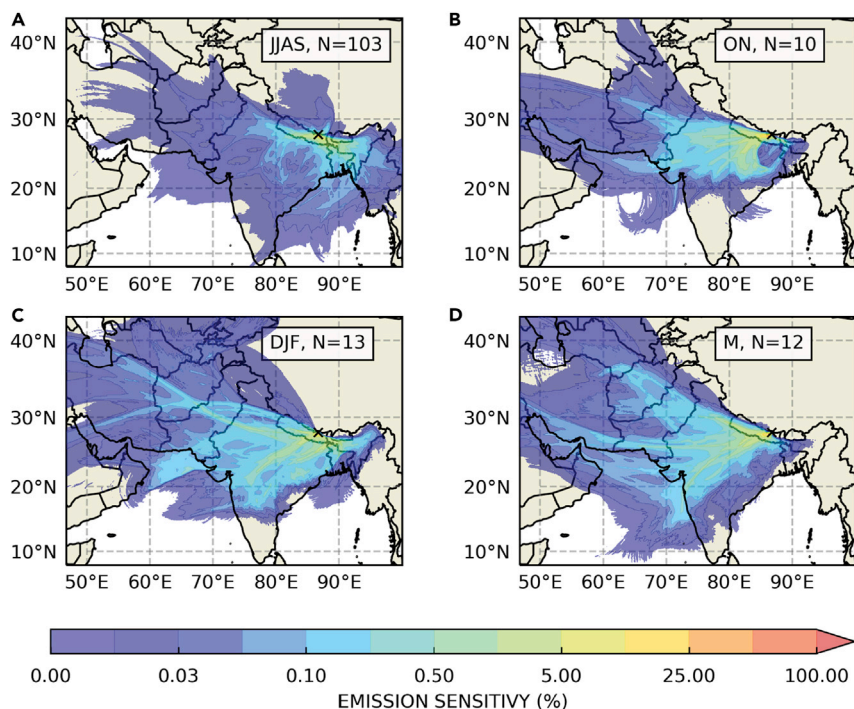


Figure 6. Seventy-two-Hour Backward Trajectories during Precipitation

Frequency (%) (see [Experimental Procedures](#)) of 72-h FLEXPART backward air trajectories ending at 650 hPa at event maturation for 2019–2020 precipitation events in Phortse for (A) JJAS, (B) ON, (C) DJF, and (D) March.

of climate change and water stress in the Khumbu and broader HKH region.

EXPERIMENTAL PROCEDURES

Resource Availability

Lead Contact

For queries related to this article, please contact perrylb@apstate.edu.

Materials Availability

No new materials were generated as a result of this research.

Data and Code Availability

The new AWS network data used for this study are available at <https://www.nationalgeographic.org/projects/perpetual-planet/everest/weather-data/>.

Precipitation data from Pheriche and Pyramid are available at <https://glacioclim.osug.fr/Donnees-himalaya>.

The code used for analysis is on GitHub: <https://github.com/heatherguy/everest-flexpart>.

Automatic Weather Stations

As part of the 2019 Everest Expedition, five weather stations were installed along an elevational transect in the Khumbu region and were described by Matthews et al.¹³ Of particular relevance for this paper, Phortse and Everest Base Camp precipitation sensors consist of two Pluvio² 1500 weighing precipitation gauges surrounded by Belfort double-alter windshields.

Table S5 summarizes the data sources and time periods used for this study. *In situ* manual daily precipitation data were obtained from the DHM for six stations in the Solo-Khumbu region ([Figure 1](#)) with a minimum of 5 years of data and completeness >80%. No records exist for stations >4,000 m asl that meet these criteria and the only two stations currently in operation are the lowest: Salleri (2,383 m asl) and Chaurikhark (2,642 m asl). The Chaurikhark record is the longest and most complete in the region, spanning 70 years with 98% completeness, although we have used only the data since 1981 due to concerns about missing data and data quality during some of the earlier years. Weighing precipitation gauges operated by the IRD and TU at Pheriche (4,260 m asl) and Pyramid (5,035 m asl; [Figure 1](#)) provided hourly precipitation data from May 2016 to November 2019. Both gauges are equipped with a single-alter windshield and data have been corrected following World Meteorological Organization recommendations⁹⁵ and successfully applied in tropical mountain environments⁷³ using a co-located RM Young 05103-5 wind sensor at the same height (~1.5 m) as the gauge, as well as Campbell Scientific CS215 temperature and relative humidity sensors.

As part of the 2019 Everest Expedition, team members installed a network of five AWSs at elevations ranging as high as 8,430 m asl¹³ ([Figure 1](#)). The lowest two AWSs, at Phortse (3,810 m asl) and Everest Base Camp (5,315 m asl), are equipped with comprehensive precipitation monitoring sensors, including OTT Pluvio² 1500-400 weighing precipitation gauges, OTT Parsivel² present weather sensors, and Campbell Scientific SR50a sonic snow depth sensors. Both Pluvio² precipitation gauges are surrounded by high-performing Belfort double-alter windshields that have demonstrated minimal under-catch of solid precipitation^{62,96} and therefore corrections are not typically needed. Although unheated tipping bucket gauges are adequate at lower elevations, <3,000 m asl, where precipitation is nearly exclusively liquid, at higher elevations they are not practical due to increased frequency of solid precipitation.^{34,97,98}

confirm the inferred moisture source regions. Additional process-based research is needed to investigate the physical mechanisms driving the nighttime maximum and vertical structure of precipitation.

In this paper we have placed the first complete year of the new AWS network in a regional and long-term context, characterized the temporal patterns and moisture source regions, and identified some key characteristics of heavy precipitation events. Our results suggest that heavy precipitation events, specific humidity, and freezing-level height have increased in the Khumbu region since 1981, with freezing-level heights rising by ~7 m year⁻¹ since 2005. Despite an anomalously late onset to the 2019 monsoon, we found that the bulk (75%–80%) of the precipitation occurs on average during the monsoon period of JJAS and falls mainly in the nighttime hours, although some altitude dependence is noted, with the winter and pre-monsoon periods of greater significance at higher elevations. We observed a nighttime precipitation maximum, peaking during the early evening at Pyramid (5,035 m asl) and close to midnight local time in Phortse (3,810 m asl), demonstrating that up- and down-valley locations in relatively close proximity exhibit dissimilar daily timing of precipitation. Important seasonal patterns are evident in the backward air trajectories associated with precipitation events, with the northern Bay of Bengal, lower Ganges and Brahmaputra basins, and Indo-Gangetic Plain serving as inferred moisture source regions during the monsoon; more westerly trajectories predominate the remainder of the year, resulting in much lower precipitation totals. Heavy precipitation events during 2019–2020 were characterized by higher mid- and upper-level moisture, large-scale ascent, and shallower lapse rates. These new findings provide an observationally based analog that contributes to informing policymakers and local communities on how to adapt to and mitigate future impacts

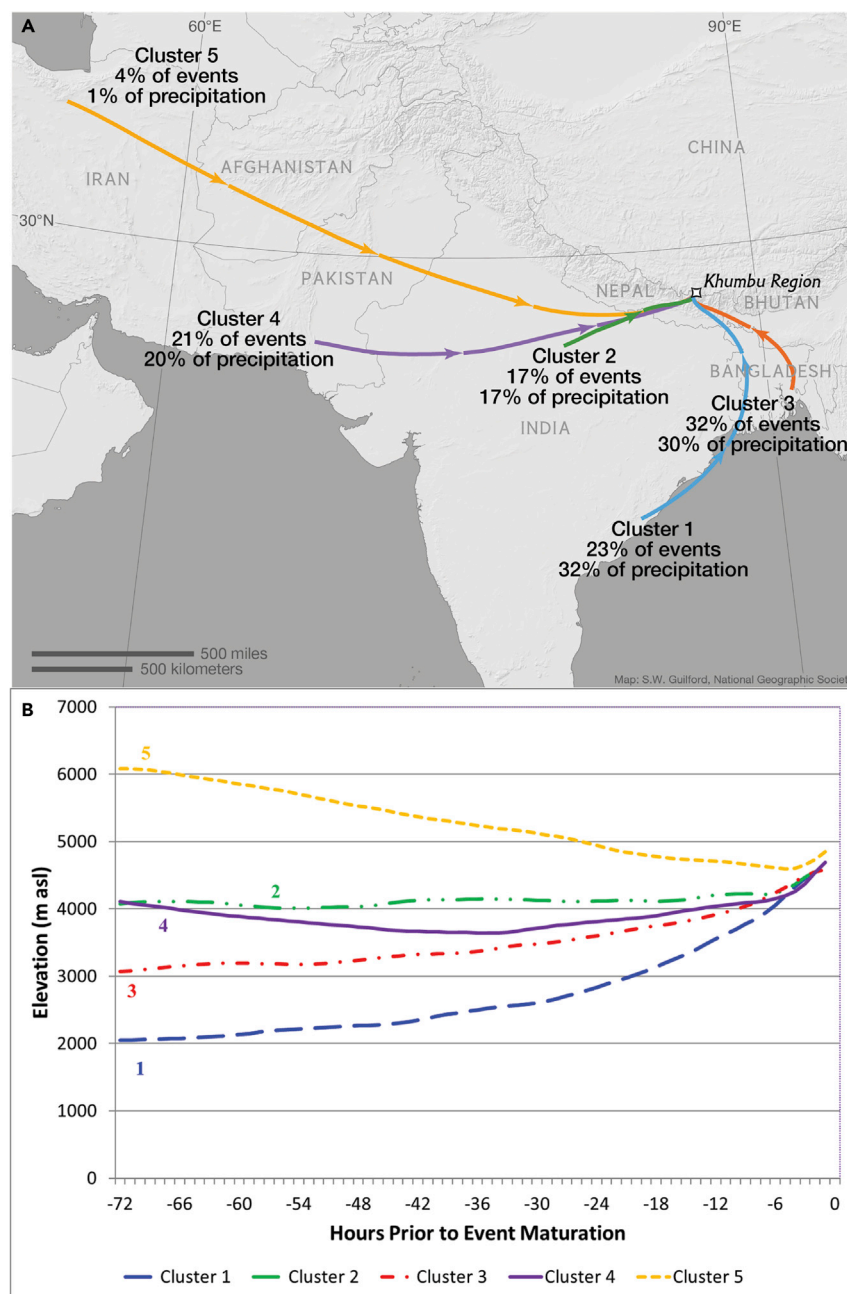


Figure 7. Khumbu Region Trajectory Cluster Analysis

(A and B) (A) Composite trajectory clusters for all 72-h FLEXPART backward trajectories ending at 650 hPa overlaid on topography and (B) vertical profiles of composite trajectory clusters for 1 June 2019 to 31 March 2020 precipitation events observed at Phortse.

determined using 1981–2019 hourly ERA5 data as the altitude of the 0°C isotherm derived using temperature and geopotential height data on pressure levels corresponding to the Phortse grid cell. We also obtained 500 hPa specific humidity data for the same time period. Additional ERA5-Single Level and Pressure Height data (Table S5) were obtained for 1 June 2019 to 31 May 2020 to complement the observations from the Phortse AWS.

Hourly precipitation data from the Phortse AWS were used to identify 171 separate precipitation events of >0.1 mm during the period 1 June 2019 to 31 May 2020 employing established approaches.^{79,101} We defined the beginning of a precipitation event as the hour measurable precipitation was first reported, the maturation of the event as the hour with the highest precipitation total, and the ending as the last hour measurable precipitation occurred. A precipitation event remained active if measurable precipitation was reported during a 6-h period; precipitation breaks over 6 h resulted in the identification of separate precipitation events. In addition to the surface meteorological data from the Phortse AWS, we included total precipitation at Pheriche, Pyramid, and Base Camp during the event. Other meteorological parameters from Camp II, South Col, and Balcony AWSs and ERA5-Single Level and Pressure Height products were likewise included in the event-level statistics. We derived lapse rates (mean value of $-5.4^{\circ}\text{C km}^{-1}$ during precipitation events) by calculating the difference in the mean temperature for each event between Phortse (3,810 m asl) and Camp II (6,464 m asl) and used this in conjunction with Phortse temperatures to estimate freezing-level heights (mean value of 4,897 m asl during precipitation events).

We used the Lagrangian particle dispersion model FLEXPART (v.10.4⁷⁰) to explore moisture source regions associated with precipitation events at Phortse between 1 June 2019 and 31 March 2020. FLEXPART is a stochastic model that computes the trajectories of a large number of infinitesimally small “particles” either backward or forward in time as the particles move with the ambient flow. The stochastic nature of FLEXPART allows for the parameterization of turbulence and convective transport within the model.

In this study, we drove FLEXPART with 3-hourly reanalysis data from ERA5,¹⁰² with $0.5^{\circ} \times 0.5^{\circ}$ horizontal resolution. At the maturation hour of each precipitation event (1 h prior to the maximum precipitation rate), we released 10,000 inert tracer particles from 86.75°E , 27.85°N , at the 650 hPa pressure level. The 650 hPa level is the approximate pressure height of Phortse and a representative endpoint for the investigation of antecedent upstream air trajectories and associated transport of low-level moisture (a 500 or 750 hPa release height produces comparable results). FLEXPART simulates the transport of each particle backward in time for 72 h prior to the release and calculates the “emission sensitivity” on a $0.1^{\circ} \times 0.1^{\circ}$ grid. The emission sensitivity for each grid cell (in units of seconds) is proportional to the total amount of time that particles have

The Parsivel² present weather sensor^{99,100} was used to classify the timing, phase, and intensity of precipitation at Phortse. Data were available for Everest Base Camp AWS only from 10 October 2019 through 31 May 2020, thereby missing the critical monsoon period of JJAS 2019. Precipitation gauges were not included on higher stations because of the considerable logistical challenges of transport, installation, and maintenance that rendered them impractical. Satellite telemetry for the Balcony AWS was lost on 20 January 2020 and redundant wind measurements at the South Col AWS failed on 5 January 2020 in an extreme windstorm.

We also obtained data from the European Centre for Medium-Range Weather Forecasts (ECMWF) ERA5-Land and ERA5-Single Level and Pressure Height products for two grid cells in the Khumbu (Figure 1). Daily precipitation totals used for the 1981–2019 trend analyses were calculated from the ERA5-Land hourly precipitation dataset. JJAS freezing-level heights were

spent in each grid cell during the simulation and is a measure of the simulated concentration at the release location that a source of unit strength (1 kg s^{-1}) in that grid cell would produce.¹⁰³ For identifying moisture source regions, we convert emission sensitivity to a percentage of the maximum value for each event that conveys the likelihood of a particle passing through each grid cell during the simulation.

To identify the key moisture transport pathways associated with precipitation events at Phortse, we calculated the mean back trajectory for each event and used the trajectory clustering algorithm implemented in the NOAA HYSPLIT (Hybrid Single Particle Lagrangian Integrated Trajectory) model⁷¹ to group the events into six clusters that represent the dominant moisture transport regimes. Due to the extremely low frequency (1.4% of total) and inconsequential mean precipitation (0.1 mm), Cluster 6 is not discussed and instead is grouped with two other unclustered trajectories in Table S3. The HYSPLIT cluster algorithm groups back trajectories together by minimizing the spatial variance within each cluster and the cluster analysis is performed on latitude and longitude and not height. The final number of clusters is the minimum number before which the sum of the spatial variances within each cluster begins to increase (indicating the merging of disparate clusters). Although there is some subjectivity involved in choosing the number of clusters to use in the cluster analysis, the large change in total spatial variance provides some objective guidance to the process and the final choice is not arbitrary.^{79,104}

Composite synoptic plots of specific humidity, wind speed, and direction were also created for 850, 500, and 300 hPa using ERA5 reanalysis data¹⁰² for Clusters 1, 2, 3, and 4. To investigate the differences in *in situ* AWS and ERA5 atmospheric parameters between heavy ($>75^{\text{th}}$ percentile) and light ($<25^{\text{th}}$ percentile) precipitation events during the monsoon, we conducted a two-sample difference of means *t* test. The non-parametric Mann-Whitney test was used for variables that did not meet statistical significance of $p < 0.01$ in the Shapiro-Wilk test for normality.

SUPPLEMENTAL INFORMATION

Supplemental Information can be found online at <https://doi.org/10.1016/j.oneear.2020.10.011>.

ACKNOWLEDGMENTS

This research was conducted in partnership with the National Geographic Society, Rolex, and Tribhuvan University, with approval from all relevant agencies of the government of Nepal. We acknowledge Conrad Anker and Peter Athans as inspirational mountaineers who prepared the 2019 Everest expedition team and kept them safe. We also wish to thank the communities of the Khumbu Region, Xtreme Climbers Treks and Expedition P. Ltd., and Jiban Ghimire and Shangri-La Nepal Trek Pvt. Ltd. We further recognize and greatly appreciate the extraordinary efforts of our entire Sherpa climbing team, whose physical and mental prowess at altitude made installation of the AWSs possible. The core AWS-installation team members were Panuru Sherpa (Sirdar), Phu Tashi Sherpa, Pemba Sherpa, Urken Lendu Sherpa, Ila Nuru Sherpa, Fura Chetten Sherpa, Lakpa Gyaljen Sherpa, Pasang Sona Sherpa, Pasang Kami Sherpa, Nima Rita Sherpa, Tenzing Gyanjen Sherpa, Nawang Phinjo Sherpa, Phinjo Sherpa, and Gyaljen Dorji Sherpa. Dawa Yangzum Sherpa and Tenzing Gyalzen Sherpa provided helpful assistance during the installations. We thank Kyler Abernathy, Mike Hughes, and Dana Greene for AWS design considerations; the team of engineers at Campbell Scientific, Inc. (Mike Hansen, Jared Campbell, Steve Gunderson, and Gary Roberts) for designing the AWSs; Sandra Elvin and Alex Tait for help during installation; and Richard Rigby for assistance in setting up and running FLEXPART. Additional funding supporting this research was provided by the National Science Foundation through grant AGS-1347179 (L.B.P.). The Pyramid and Pheriche stations have been funded by the French Service d'Observation GLACIOCLIM (part of IR OZCAR) and by a grant from Labex OSUG@2020 (Investissements d'avenir – ANR10 LABX56) and have been operated with the support of the JEA1 HIMALICE and the Ev-K2-CNR Project in collaboration with the Nepal Academy of Science and Technology and Tribhuvan University. We also thank three anonymous reviewers for their helpful comments.

AUTHOR CONTRIBUTIONS

Conceptualization, L.B.P. and T.M.; Investigation, L.B.P., T.M., H.G., and A.K.; Methodology, L.B.P., T.M., and H.G.; Resources, L.B.P., T.M., A.C.E., D.S., S.T., S.B., P.W., I.K., A.K., and D.A.; Software, T.M. and H.G.; Visualization, L.B.P., T.M., and H.G.; Writing – Original Draft, L.B.P.; Writing – Reviewing & Editing, L.B.P., T.M., H.G., I.K., D.S., A.C.E., A.C.E., P.W., A.S., A.P.G., and P.A.M.

DECLARATION OF INTERESTS

The authors declare no competing interests.

Received: July 31, 2020

Revised: October 13, 2020

Accepted: October 26, 2020

Published: November 20, 2020

REFERENCES

- Immerzeel, W.W., Lutz, A.F., Andrade, M., Bahl, A., Biemans, H., Bolch, T., Hyde, S., Brumby, S., Davies, B.J., Elmore, A.C., et al. (2020). Importance and vulnerability of the world's water towers. *Nature* 577, 364–369.
- Pritchard, H.D. (2019). Asia's shrinking glaciers protect large populations from drought stress. *Nature* 569, 649–654.
- Wester, P., Mishra, A., Mukherji, A., and Shrestha, A.B. (2019). The Hindu Kush Himalaya Assessment: Mountains, Climate Change, Sustainability and People (Springer International Publishing).
- Wood, L.R., Neumann, K., Nicholson, K.N., Bird, B.W., Dowling, C.B., and Sharma, S. (2020). Melting Himalayan glaciers threaten domestic water resources in the mount everest region, Nepal. *Front. Earth Sci.* 8, 1–8.
- Biemans, H., Siderius, C., Lutz, A.F., Nepal, S., Ahmad, B., Hassan, T., von Bloh, W., Wijngaard, R.R., Wester, P., Shrestha, A.B., et al. (2019). Importance of snow and glacier meltwater for agriculture on the Indo-Gangetic Plain. *Nat. Sustain.* 2, 594–601.
- Lutz, A.F., Immerzeel, W.W., Shrestha, A.B., and Bierkens, M.F.P. (2014). Consistent increase in High Asia's runoff due to increasing glacier melt and precipitation. *Nat. Clim. Chang.* 4, 587–592.
- Bolch, T., Shea, J.M., Liu, S., Azam, F.M., Gao, Y., Gruber, S., Immerzeel, W.W., Kulkarni, A., Li, H., Tahir, A.A., et al. (2019). Status and change of the cryosphere in the extended Hindu Kush Himalaya Region. In *The Hindu Kush Himalaya Assessment*, P. Wester, A. Mishra, A. Mukherji, and A. Shrestha, eds. (Springer), pp. 209–255.
- Maurer, J.M., Schaefer, J.M., Rupper, S., and Corley, A. (2019). Acceleration of ice loss across the Himalayas over the past 40 years. *Sci. Adv.* 5, eaav7266.
- Soncini, A., Bocchiola, D., Confortola, G., Minora, U., Vuillermoz, E., Salerno, F., Viviano, G., Shrestha, D., Senese, A., Smiraglia, C., et al. (2016). Future hydrological regimes and glacier cover in the Everest region: the case study of the upper Dudh Koshi basin. *Sci. Total Environ.* 565, 1084–1101.
- Panday, P.K., Thibeault, J., and Frey, K.E. (2015). Changing temperature and precipitation extremes in the Hindu Kush-Himalayan region: an analysis of CMIP3 and CMIP5 simulations and projections. *Int. J. Climatol.* 35, 3058–3077.
- Bookhagen, B., and Burbank, D.W. (2010). Toward a complete Himalayan hydrological budget: spatiotemporal distribution of snowmelt and rainfall and their impact on river discharge. *J. Geophys. Res. Earth Surf.* 115, <https://doi.org/10.1029/2009JF001426>.
- Sunako, S., Fujita, K., Sakai, A., and Kayastha, R.B. (2019). Mass balance of Trambau Glacier, Rolwaling region, Nepal Himalaya: in-situ observations, long-term reconstruction and mass-balance sensitivity. *J. Glaciol.* 65, 605–616.

13. Matthews, T., Perry, L.B., Koch, I., Aryal, D., Khadka, A., Shrestha, D., Abernathy, K., Elmore, A.C., Seimon, A., Tait, A., et al. (2020). Going to extremes: installing the world's highest weather stations on Mount Everest. *Bull. Am. Meteorol. Soc.* 1–44, <https://doi.org/10.1175/BAMS-D-19-0198.1>.
14. Shea, J.M., Wagnon, P., Immerzeel, W.W., Biron, R., Brun, F., and Pellicciotti, F. (2015). A comparative high-altitude meteorological analysis from three catchments in the Nepalese Himalaya. *Int. J. Water Resour. Dev.* 31, 174–200.
15. Hock, R., Rasul, G., Adler, C., Cáceres, B., Gruber, S., Hirabayashi, Y., Jackson, M., Kääb, A., Kang, S., Kutuzov, S., et al. (2019). Chapter 2: high mountain areas. IPCC special report on the ocean and cryosphere in a changing climate. IPCC Spec. Rep. Ocean Cryosph. A Chang. Clim. 131–202.
16. Wijngaard, R.R., Lutz, A.F., Nepal, S., Khanal, S., Pradhananga, S., Shrestha, A.B., and Immerzeel, W.W. (2017). Future changes in hydro-climatic extremes in the upper Indus, Ganges, and Brahmaputra river basins. *PLoS One* 12, e0190224.
17. Miner, K.R., Mayewski, P.A., Baidya, S.K., Broad, K., Clifford, H., Gajurel, A., Bibek, G., Hubbard, M., Jaskolski, C., Koldewey, H., et al. Emergent risks in the Mt. Everest region in the time of anthropogenic change. *One Earth* 88 <https://doi.org/10.5281/zenodo.3972343>
18. Aubriot, O., Faulon, M., Sacareau, I., Puschiasis, O., Jacquemet, E., Smadja, J., André-Lamat, V., Abadia, C., and Muller, A. (2019). Reconfiguration of the water–energy–food nexus in the Everest tourist region of Solukhumbu, Nepal. *Mt. Res. Dev.* 39, R47–R59.
19. Sharma, S., Khadka, N., Hamal, K., and Shrestha, D. (2020). How accurately can satellite products (TMPA and IMERG) detect precipitation patterns, extremities, and drought across the Nepalese Himalaya? *Earth Space Sci.* 7, <https://doi.org/10.1029/2020EA001315>.
20. Hamal, K., Sharma, S., Khadka, N., Baniya, B., Ali, M., Shrestha, M.S., Xu, T., Shrestha, D., and Dawadi, B. (2020). Evaluation of MERRA-2 precipitation products using gauge observation in Nepal. *Hydrology* 7, 40.
21. Salerno, F., Guyennon, N., Thakuri, S., Viviano, G., Romano, E., Vuillermoz, E., Cristofanelli, P., Stocchi, P., Agrillo, G., Ma, Y., et al. (2015). Weak precipitation, warm winters and springs impact glaciers of south slopes of Mt. Everest (central Himalaya) in the last 2 decades (1994–2013). *Cryosphere* 9, 1229–1247.
22. Yamamoto, M.K., Ueno, K., and Nakamura, K. (2011). Comparison of satellite precipitation products with rain gauge data for the Khumbu Region, Nepal Himalayas. *J. Meteorol. Soc. Jpn.* 89, 597–610.
23. Barros, A.P., and Lang, T.J. (2003). Monitoring the monsoon in the Himalayas: observations in Central Nepal, June 2001. *Mon. Weather Rev.* 131, 1408–1427.
24. Barros, A.P., Joshi, M., Putkonen, J., and Burbank, D.W. (2000). A study of 1999 monsoon rainfall in a mountainous region in central Nepal using TRMM products and rain gauge observations. *Geophys. Res. Lett.* 27, 3683–3686.
25. Bhatt, B.C., and Nakamura, K. (2005). Characteristics of monsoon rainfall around the Himalayas revealed by TRMM precipitation radar. *Mon. Weather Rev.* 133, 149–165.
26. Bhatt, B.C., and Nakamura, K. (2006). A climatological-dynamical analysis associated with precipitation around the southern part of the Himalayas. *J. Geophys. Res. Atmos.* 111, 1–13.
27. Yang, K., Guyennon, N., Ouyang, L., Tian, L., Tartari, G., and Salerno, F. (2018). Impact of summer monsoon on the elevation-dependence of meteorological variables in the south of central Himalaya. *Int. J. Climatol.* 38, 1748–1759.
28. Ouyang, L., Yang, K., Lu, H., Chen, Y., Lazhu, Zhou, X., and Wang, Y. (2020). Ground-based observations reveal unique valley precipitation patterns in the Central Himalaya. *J. Geophys. Res. Atmos.* 125, 1–18.
29. Eeckman, J., Chevallier, P., Boone, A., Neppel, L., De Rouw, A., Delclaux, F., and Koiraal, D. (2017). Providing a non-deterministic representation of spatial variability of precipitation in the Everest region. *Hydrol. Earth Syst. Sci.* 21, 4879–4893.
30. Shrestha, D., Singh, P., and Nakamura, K. (2012). Spatiotemporal variation of rainfall over the central Himalayan region revealed by TRMM Precipitation Radar. *J. Geophys. Res. Atmos.* 117, 1–14.
31. Bookhagen, B., and Burbank, D.W. (2006). Topography, relief, and TRMM-derived rainfall variations along the Himalaya. *Geophys. Res. Lett.* 33, 1–5.
32. Seko, K. (1987). Seasonal variation of altitudinal dependence of precipitation in Langtang Valley, Nepal Himalayas. *Bull. Glaciol. Res.* 5, 41–47.
33. Sherpa, S.F., Wagnon, P., Brun, F., Berthier, E., Vincent, C., Lejeune, Y., Arnaud, Y., Kayastha, R.B., and Sinisalo, A. (2017). Contrasted surface mass balances of debris-free glaciers observed between the southern and the inner parts of the Everest region (2007–15). *J. Glaciol.* 63, 637–651.
34. Saloranta, T., Thapa, A., Kirkham, J.D., Koch, I., Melvold, K., Stigter, E., Litt, M., and Møen, K. (2019). A model setup for mapping snow conditions in high-mountain Himalaya. *Front. Earth Sci.* 7, 1–18.
35. Hunt, K.M.R., and Fletcher, J.K. (2019). The relationship between Indian monsoon rainfall and low-pressure systems. *Clim. Dyn.* 53, 1859–1871.
36. Zhang, Z., Chan, J.C.L., and Ding, Y. (2004). Characteristics, evolution and mechanisms of the summer monsoon onset over Southeast Asia. *Int. J. Climatol.* 24, 1461–1482.
37. Dhar, O.N., and Nandargi, S. (2000). An appraisal of precipitation distribution around the Everest and Kanchenjunga peaks in the Himalayas. *Weather* 55, 223–234.
38. Hunt, K.M.R., Turner, A.G., Inness, P.M., Parker, D.E., and Levine, R.C. (2016). On the structure and dynamics of Indian monsoon depressions. *Mon. Weather Rev.* 144, 3391–3416.
39. Molley, D.A., and Shukla, J. (1989). Main features of the westward-moving low pressure systems which form over the Indian region during the summer monsoon and relation to the monsoon rainfall. *Mausam* 40, 137–152.
40. Romatschke, U., and Houze, R.A. (2011). Characteristics of precipitating convective systems in the South Asian monsoon. *J. Hydrometeorol.* 12, 3–26.
41. Bollasina, M.A., Bertolani, L., and Tartari, G. (2002). Meteorological observations at high altitude in the Khumbu valley, Nepal Himalayas, 1994–1999. *Bull. Glaciol. Res.* 19, 1–11.
42. Bohlinger, P., Sorteberg, A., and Sodemann, H. (2017). Synoptic conditions and moisture sources actuating extreme precipitation in Nepal. *J. Geophys. Res. Atmos.* 122, 12,653–12,671.
43. Cong, Z., Kang, S., and Qin, D. (2009). Seasonal features of aerosol particles recorded in snow from Mt. Qomolangma (Everest) and their environmental implications. *J. Environ. Sci.* 21, 914–919.
44. Dahal, R.K., and Hasegawa, S. (2008). Representative rainfall thresholds for landslides in the Nepal Himalaya. *Geomorphology* 100, 429–443.
45. Chhetri, T.B., Dhital, Y.P., Tandong, Y., Devkota, L.P., and Dawadi, B. (2020). Observations of heavy rainfall and extreme flood events over Banke-Bardiya districts of Nepal in 2016–2017. *Prog. Disaster Sci.* 6, 100074.
46. Dhar, O.N., and Nandargi, S. (2003). Hydrometeorological aspects of floods in India. *Nat. Hazards* 28, 1–33.
47. Immerzeel, W.W., Wanders, N., Lutz, A.F., Shea, J.M., and Bierkens, M.F.P. (2015). Reconciling high-altitude precipitation in the upper Indus basin with glacier mass balances and runoff. *Hydrol. Earth Syst. Sci.* 19, 4673–4687.
48. Simon Wang, S.-Y., Gillies, R.R., Fosu, B., and Singh, P.M. (2016). The deadly Himalayan snowstorm of October 2014: synoptic conditions and associated trends. *Bull. Am. Meteorol. Soc.* 96, S89–S94.
49. Ueno, K., Kayastha, R.B., Chitrakar, M.R., Bajracharya, O.R., Pokhrel, A.P., Fujinami, H., Kadota, T., Iida, H., Manandhar, D.P., Hattori, M., et al. (2001). Meteorological observations during 1994–2000 at the

- automatic weather station (GEN-AWS) in Khumbu region, Nepal Himalayas. *Bull. Glaciol. Res.* **18**, 23–30.
50. Bonekamp, P.N.J., de Kok, R.J., Collier, E., and Immerzeel, W.W. (2019). Contrasting meteorological drivers of the glacier mass balance between the Karakoram and central Himalaya. *Front. Earth Sci.* **7**, 1–14.
51. Romatschke, U., and Houze, R.A. (2011). Characteristics of precipitating convective systems in the premonsoon season of South Asia. *J. Hydrometeorol.* **12**, 157–180.
52. Krishnan, R., Shrestha, A.B., Ren, G., Rajbhandari, R., Saeed, S., Sanjay, J., et al. (2019). Unravelling climate change in the Hindu Kush Himalaya: rapid warming in the mountains and increasing extremes BT. In the Hindu Kush Himalaya assessment: mountains, climate change, sustainability and people, P. Wester, A. Mishra, A. Mukherji, and A.B. Shrestha, eds. (Springer International Publishing), pp. 57–97.
53. Pokharel, B., Wang, S.Y.S., Meyer, J., Marahatta, S., Nepal, B., Chikamoto, Y., and Gillies, R. (2020). The east–west division of changing precipitation in Nepal. *Int. J. Climatol.* **40**, 3348–3359.
54. Palazzi, E., Von Hardenberg, J., and Provenzale, A. (2013). Precipitation in the hindu-kush karakoram himalaya: observations and future scenarios. *J. Geophys. Res. Atmos.* **118**, 85–100.
55. Hartmann, D.L., Klein Tank, A.M.G., Rusticucci, M., Alexander, L.V., Brönnimann, S., Charabi, Y.A.R., Dentener, F.J., Dlugokencky, E.J., Easterling, D.R., Kaplan, A., et al. (2013). Observations: atmosphere and surface. *Clim. Chang.* 2013 Phys. Sci. Basis Work. Gr. I Contrib. Fifth Assess. Rep. Intergov. Panel Clim. Chang. **9781107057**, 159–254.
56. Karki, R., Hasson, S., Schickhoff, U., Scholten, T., and Böhner, J. (2017). Rising precipitation extremes across Nepal. *Climate* **5**, 1–25.
57. Pepin, N., Bradley, R.S., Diaz, H.F., Baraer, M., Caceres, E.B., Forsythe, N., Fowler, H., Greenwood, G., Hashmi, M.Z., Liu, X.D., et al. (2015). Elevation-dependent warming in mountain regions of the world. *Nat. Clim. Chang.* **5**, 424–430.
58. Thakuri, S., Salerno, F., Smiraglia, C., Bolch, T., D’Agata, C., Viviano, G., and Tartari, G. (2014). Tracing glacier changes since the 1960s on the south slope of Mt. Everest (central Southern Himalaya) using optical satellite imagery. *Cryosphere* **8**, 1297–1315.
59. Shrestha, A.B., Wake, C.P., Mayewski, P.A., and Dibb, J.E. (1999). Maximum temperature trends in the Himalaya and its vicinity: an analysis based on temperature records from Nepal for the period 1971–94. *J. Clim.* **12**, 2775–2786.
60. Thakuri, S., Dahal, S., Shrestha, D., Guyennon, N., Romano, E., Colombo, N., and Salerno, F. (2019). Elevation-dependent warming of maximum air temperature in Nepal during 1976–2015. *Atmos. Res.* **228**, 261–269.
61. Rajbhandari, R., Shrestha, A.B., Nepal, S., and Wahid, S. (2016). Projection of future climate over the koshi river basin based on CMIP5 GCMs. *Atmos. Clim. Sci.* **06**, 190–204.
62. Rasmussen, R., Baker, B., Kochendorfer, J., Meyers, T., Landolt, S., Fischer, A.P., Black, J., Thériault, J.M., Kucera, P., Gochis, D., et al. (2012). How well are we measuring snow: the NOAA/FAA/NCAR winter precipitation test bed. *Bull. Am. Meteorol. Soc.* **93**, 811–829.
63. Barry, R.G. (2008). *Mountain Weather and Climate*, Third Edition (Cambridge University Press).
64. Francou, B., Vuille, M., Wagnon, P., Mendoza, J., and Sicart, J.-E. (2003). Tropical climate change recorded by a glacier in the central Andes during the last decades of the twentieth century: Chacaltaya, Bolivia, 16°S. *J. Geophys. Res. Atmos.* **108**, <https://doi.org/10.1029/2002JD002959>.
65. Schwanghart, W., Worni, R., Huggel, C., Stoffel, M., and Korup, O. (2016). Uncertainty in the Himalayan energy–water nexus: estimating regional exposure to glacial lake outburst floods. *Environ. Res. Lett.* **11**, 74005.
66. Litt, M., Shea, J., Wagnon, P., Steiner, J., Koch, I., Stigter, E., and Immerzeel, W. (2019). Glacier ablation and temperature indexed melt models in the Nepalese Himalaya. *Sci. Rep.* **9**, 1–13.
67. Kanda, N., Negi, H.S., Rishi, M.S., and Kumar, A. (2020). Performance of various gridded temperature and precipitation datasets over Northwest Himalayan Region. *Environ. Res. Commun.* **2**, 085002.
68. Orsolini, Y., Wegmann, M., Dutra, E., Liu, B., Balsamo, G., Yang, K., De Rosnay, P., Zhu, C., Wang, W., Senan, R., et al. (2019). Evaluation of snow depth and snow cover over the Tibetan Plateau in global reanalyses using in situ and satellite remote sensing observations. *Cryosphere* **13**, 2221–2239.
69. Zhu, Y.Y., and Yang, S. (2020). Evaluation of CMIP6 for historical temperature and precipitation over the Tibetan Plateau and its comparison with CMIP5. *Adv. Clim. Chang. Res.* **1–13**, <https://doi.org/10.1016/j.accres.2020.08.001>.
70. Pissio, I., Sollum, E., Grythe, H., Kristiansen, N.I., Cassiani, M., Eckhardt, S., Arnold, D., Morton, D., Thompson, R.L., Groot Zwaftink, C.D., et al. (2019). The Lagrangian particle dispersion model FLEXPART version 10.4. *Geosci. Model Dev.* **12**, 4955–4997.
71. Stein, A.F., Draxler, R.R., Rolph, G.D., Stunder, B.J.B., Cohen, M.D., and Ngan, F. (2015). NOAA’s hysplit atmospheric transport and dispersion modeling system. *Bull. Am. Meteorol. Soc.* **96**, 2059–2077.
72. Junquas, C., Takahashi, K., Condom, T., Espinoza, J.C., Chavez, S., Sicart, J.E., and Lebel, T. (2018). Understanding the influence of orography on the precipitation diurnal cycle and the associated atmospheric processes in the central Andes. *Clim. Dyn.* **50**, 3995–4017.
73. Wagnon, P., Lafaysse, M., Lejeune, Y., Maisincho, L., Rojas, M., and Chazarin, J.P. (2009). Understanding and modeling the physical processes that govern the melting of snow cover in a tropical mountain environment in Ecuador. *J. Geophys. Res. Atmos.* **114**, 1–14.
74. Seneviratne, S.I., Nicholls, N., Easterling, D., Goodess, C.M., Kanae, S., Kossin, J., Luo, Y., Marengo, J., Mc Innes, K., Rahimi, M., et al. (2012). Changes in climate extremes and their impacts on the natural physical environment. *Manag. Risks Extrem. Events Disasters Adv. Clim. Chang. Adapt. Spec. Rep. Intergov. Panel Clim. Chang.* **9781107025**, 109–230.
75. Nepal, G. (2020). Monsoon Onset and Withdrawal Date Information (Government of Nepal, Department of Hydrology and Meteorology). nepalindata.com.
76. Khadka, A., Matthews, T., Perry, L.B., Koch, I., Wagnon, P., Shrestha, D., et al. (2020). Weather on Mount Everest during the 2019 Summer Monsoon (Weather Preprint). http://climate.appstate.edu/~perrylb/Pubs/Preprints/Khadka_et_al_2020_preprint.pdf.
77. Kirkham, J.D., Koch, I., Saloranta, T.M., Litt, M., Stigter, E.E., Møen, K., Thapa, A., Melvold, K., and Immerzeel, W.W. (2019). Near real-time measurement of snow water equivalent in the Nepal Himalayas. *Front. Earth Sci.* **7**, 1–18.
78. Chavez, S.P., and Takahashi, K. (2017). Orographic rainfall hot spots in the Andes–Amazon transition according to the TRMM precipitation radar and in situ data. *J. Geophys. Res.* **122**, 5870–5882.
79. Perry, L.B., Seimon, A., and Kelly, G.M. (2014). Precipitation delivery in the tropical high Andes of southern Peru: new findings and paleoclimatic implications. *Int. J. Climatol.* **34**, 197–215.
80. Perry, L.B., Seimon, A., Andrade-Flores, M.F., Endries, J.L., Yuter, S.E., Velarde, F., Arias, S., Bonshoms, M., Burton, E.J., Winkelmann, I.R., et al. (2017). Characteristics of precipitating storms in glacierized tropical andean cordilleras of Peru and Bolivia. *Ann. Am. Assoc. Geogr.* **107**, 309–322.
81. Bendix, J., Rollenbeck, R., and Reudenbach, C. (2006). Diurnal patterns of rainfall in a tropical Andean valley of southern Ecuador as seen by a vertically pointing K-band Doppler radar. *Int. J. Climatol.* **26**, 829–846.
82. Xu, W., and Zipser, E.J. (2011). Diurnal variations of precipitation, deep convection, and lightning over and east of the eastern Tibetan Plateau. *J. Clim.* **24**, 448–465.
83. Collier, E., and Immerzeel, W.W. (2015). High-resolution modeling of atmospheric dynamics in the Nepalese Himalaya. *J. Geophys. Res. Atmos.* **120**, 9882–9896.

84. Matthews, T., Murphy, C., McCarthy, G., Broderick, C., and Wilby, R.L. (2018). Super storm Desmond: a process-based assessment. *Environ. Res. Lett.* **13**, 014024.
85. Khan, T.M.A., Quadir, D.A., Murty, T.S., and Sarker, M.A. (2004). Seasonal and interannual sea surface temperature variability in the coastal cities of Arabian Sea and Bay of Bengal. *Nat. Hazards* **31**, 549–560.
86. de Kok, R.J., Tuinenburg, O.A., Bonekamp, P.N.J., and Immerzeel, W.W. (2018). Irrigation as a potential driver for anomalous glacier behavior in High Mountain Asia. *Geophys. Res. Lett.* **45**, 2047–2054.
87. Perry, L.B., Yuter, S.E., Matthews, T., Wagnon, P., Khadka, A., Aryal, D., Shrestha, D., Tait, A., Miller, M.A., O'Neill, A., et al. (2020). Direct observations of a Mt. Everest snowstorm from the world's highest surface-based radar observations. *Weather Early View*. <https://doi.org/10.1002/wea.3854>.
88. Srivastava, A.K., Ram, K., Pant, P., Hegde, P., and Joshi, H. (2012). Black carbon aerosols over Manora Peak in the Indian Himalayan foothills: implications for climate forcing. *Environ. Res. Lett.* **7**, 014002.
89. Mahmood, R., Pielke, R.A., Hubbard, K.G., Niyogi, D., Dirmeyer, P.A., Mcalpine, C., Carleton, A.M., Hale, R., Gameda, S., Beltrán-Przekurat, A., et al. (2014). Land cover changes and their biogeophysical effects on climate. *Int. J. Climatol.* **34**, 929–953.
90. Bell, S.S., Chand, S.S., Tory, K.J., Ye, H., and Turville, C. North Indian Ocean tropical cyclone activity in CMIP5 experiments: future projections using a model-independent detection and tracking scheme. *Int. J. Climatol.*, <https://doi.org/10.1002/joc.6594>
91. Knutson, T., Camargo, S.J., Chan, J.C.L., Emanuel, K., Ho, C.H., Kossin, J., Mohapatra, M., Satoh, M., Sugi, M., Walsh, K., et al. (2020). Tropical cyclones and climate change assessment. *Bull. Am. Meteorol. Soc.* **100**, 1987–2007.
92. Walsh, K.J.E., McBride, J.L., Klotzbach, P.J., Balachandran, S., Camargo, S.J., Holland, G., Knutson, T.R., Kossin, J.P., Lee, T., Cheung, et al. (2016). Tropical cyclones and climate change. *Wiley Interdiscip. Rev. Clim. Chang.* **7**, 65–89.
93. Kattelman, R., and Yamada, T. (1996). Case Histories Storms and Avalanches of November 1995, Khumbu Himal, Nepal. In *Proceedings of the 1996 International Snow Science Workshop, Banff, Canada*. Montana State University Library.
94. Sodemann, H., Schwierz, C., and Wernli, H. (2008). Interannual variability of Greenland winter precipitation sources: Lagrangian moisture diagnostic and North Atlantic Oscillation influence. *J. Geophys. Res. Atmos.* **113**, <https://doi.org/10.1029/2007JD008503>.
95. Førland, E.J., Allerup, P., Dahlström, B., Elomaa, E., Jonsson, T., Madsen, H., Perälä, J., Rissanen, P., Vedin, H., and Vejen, F. (1996). Manual for operational correction of Nordic precipitation data. *Nor. Meteorol. Inst.* **72**, Norske Meteorologiske Institutt.
96. Kochendorfer, J., Earle, M.E., Hodyss, D., Reverdin, A., Roulet, Y.A., Nitu, R., Rasmussen, R., Landolt, S., Buisán, S., and Laine, T. (2020). Undercatch adjustments for tipping-bucket gauge measurements of solid precipitation. *J. Hydrometeorol.* **21**, 1193–1205.
97. Wagnon, P., Vincent, C., Arnaud, Y., Berthier, E., Vuilleumoz, E., Gruber, S., Ménégoz, M., Gilbert, A., Dumont, M., Shea, J.M., et al. (2013). Seasonal and annual mass balances of Mera and Pokalde glaciers (Nepal Himalaya) since 2007. *Cryosphere* **7**, 1769–1786.
98. Karki, R. (2012). Intercomparison of Snowfall Measured by Weighing and Tipping Bucket Precipitation Gauges at Jumla Airport, Nepal, 9. https://www.wmo.int/pages/prog/www/IMOP/publications/IOM-109_TECO-2012/Session2/O2_02_Karki_Intercomparison_of_Snowfall_Measurements_Nepal.pdf.
99. Löffler-Mang, M., and Joss, J. (2000). An optical disdrometer for measuring size and velocity of hydrometeors. *J. Atmos. Ocean. Technol.* **17**, 130–139.
100. Löffler-Mang, M., and Blahak, U. (2001). Estimation of the equivalent radar reflectivity factor from measured snow size spectra. *J. Appl. Meteorol.* **40**, 843–849.
101. Perry, L.B., Konrad, C.E., and Schmidlin, T.W. (2007). Antecedent upstream air trajectories associated with northwest flow snowfall in the Southern Appalachians. *Weather Forecast.* **22**, 334–352.
102. Hersbach, H., Bell, B., Berrisford, P., Hirahara, S., Horányi, A., Muñoz-Sabater, J., Nicolas, J., Peubey, C., Radu, R., Schepers, D., et al. (2020). The ERA5 global reanalysis. *Q. J. R. Meteorol. Soc.* **146**, 1999–2049.
103. Seibert, P., and Frank, A. (2004). Source-receptor matrix calculation with a Lagrangian particle dispersion model in backward mode. *Atmos. Chem. Phys.* **4**, 51–63.
104. Taubman, B.F., Hains, J.C., Thompson, A.M., Marufu, L.T., Doddridge, B.G., Stehr, J.W., Piety, C.A., and Dickerson, R.R. (2006). Aircraft vertical profiles of trace gas and aerosol pollution over the mid-Atlantic United States: Statistics and meteorological cluster analysis. *J. Geophys. Res. Atmos.* **111**, <https://doi.org/10.1029/2005JD006196>.